

Simulation of the initial polarization curves and hysteresis loops for ferroelectric films by an extensive time-dependent Ginzburg–Landau model

Ying-Long Wang · Xing-Yuan Wang · Li-Zhi Chu · Ze-Chao Deng ·
Xue-Cheng Ding · Wei-Hua Liang · Peng-Cheng Zhang · Lin Liu ·
Bao-Ting Liu · Guang-Sheng Fu

Received: 1 September 2010 / Accepted: 2 December 2010 / Published online: 16 December 2010
© Springer Science+Business Media, LLC 2010

Abstract The polarization hysteresis loops as well as the initial curves of ferroelectric films with 180° domain boundaries perpendicular to the film surface are simulated based on an extensive time-dependent Ginzburg–Landau model. The result shows that the curve and loop strongly depend on the frequency ω of the applied electric field, the effective mass density ρ , and the viscosity coefficient K of the material, however, the constant $\omega K/\rho$ can induce the same curve and loop. The hysteresis area of the saturated loop is increased with field amplitude, which is consistent with the previous experimental observation. In addition, it is found that the latent domains in the film can result in a remarkable decrease in the remanent polarization and coercive field.

Introduction

Ferroelectric materials characterizing bistable property have attracted increasing attention in recent years [1–10] for their applications in nonvolatile random access memories, tunable microwave devices, and microelectromechanical systems [1–6]. In order to improve the performance of these ferroelectric devices, it is of wide interest and great importance to investigate the dynamic hysteresis characteristics of ferroelectric materials under various conditions, such as different frequencies and amplitudes of applied electric fields, defect

distribution in the ferroelectrics. The frequency dependence has been measured very carefully experimentally since 1995 [11]. Both the coercive field E_c , the remanent polarization P_r , and thus hysteresis loop area $\langle A \rangle$ change significantly between kHz frequencies and MHz frequencies [12, 13]. It has been observed that an increase in the frequency produces a continuous increase in the coercive field [14–16] for low frequency. And the experiment on the soft lead zirconate titanate (PZT) bulk ceramics approves that hysteresis area $\langle A \rangle$ increases with the increase of field amplitude E_0 [17]. The influence of the defects (space charges [18, 19] and dipolar defects [20, 21]) on the ferroelectric hysteretic behaviors has been investigated experimentally. The results show that they result in the lower polarization and coercive field than those of defect-free case [22–28].

Theoretically, there are many attempts to model the hysteretic loops (P – E curves) [12, 13, 29–33], which are directly related to the switching behavior of ferroelectric polarization. This attempt is believed very difficult because the switching process is nonlinear and history dependent; consequently, existing models use either oversimplified expressions that are insufficient for the unsaturated loops or complicated mathematical description that has unapparent physical meaning. Wang et al. [34] have proposed a time-dependent model by incorporating an effective kinetic energy term with the Landau free energy expansion, and the time-dependent polarization and electric-field distribution during domain switching process in ferroelectric films are calculated. In this model, a material parameter ρ having the meaning of effective mass density and another viscosity coefficient K related to the domain-wall mobility are introduced. This model is fit for the saturated as well as the unsaturated cases, in which the initial nucleation and growth of the ferroelectric domain are distinctly demonstrated. However, the ferroelectric hysteretic loops are not simulated in that article [34].

Y.-L. Wang (✉) · X.-Y. Wang · L.-Z. Chu · Z.-C. Deng ·
X.-C. Ding · W.-H. Liang · P.-C. Zhang · L. Liu · B.-T. Liu ·
G.-S. Fu (✉)
College of Physics Science and Technology, Hebei University,
Baoding 071002, People's Republic of China
e-mail: hdwangyl@hbu.edu.cn

G.-S. Fu
e-mail: fugs@hbu.edu.cn

As already known, when an electric field is applied to a ferroelectric material in the virgin state, the polarization would increase first with the applied field until reaching the saturation state, corresponding to the initial polarization of a ferroelectric material, and then the polarization would change to form the P – E loop. Although the time response of the switching fraction under a constant field has been investigated [35], no article on the theoretical study of the initial polarization curves is published.

In this article, based on the extensive time-dependent Ginzburg–Landau model, the polarization hysteresis loops as well as the initial curves of ferroelectric films with 180° domain boundaries perpendicular to the film surface are simulated. The influence of the frequency ω of the applied electric field, the effective mass density ρ , the viscosity coefficient K and the latent domain (non-switchable domain) of the material on the initial polarization curve and loop is discussed. At the same time, the hysteresis area of the loop versus the frequency, field amplitude and latent domain percentage is obtained.

Model

The free energy of a ferroelectric thin film with the dimension $x \times y \times z = L_x \times L_y \times h$, with polarization P along with z axis, is given by [34].

$$\begin{aligned} F = & \iiint_V \left\{ \frac{A}{2} P^2 + \frac{B}{4} P^4 + \frac{C}{6} P^6 + \frac{D_{11}}{2} \left(\frac{\partial P}{\partial z} \right)^2 \right. \\ & + \frac{D_{44}}{2} \left[\left(\frac{\partial P}{\partial x} \right)^2 + \left(\frac{\partial P}{\partial y} \right)^2 \right] - \frac{1}{2} E_d P - E_{\text{ext}} P - 2\sigma_r Q P^2 \Big\} dV \\ & + \iint_{S_1} \frac{D_{11} \delta_3^{-1}}{2} P^2 dx dy \\ & + \iint_{S_2} \frac{D_{44} \delta_1^{-1}}{2} P^2 dy dz + \iint_{S_3} \frac{D_{44} \delta_1^{-1}}{2} P^2 dx dz \\ & + \frac{1}{2} \rho \left(\frac{\partial P}{\partial t} \right)^2, \end{aligned} \quad (1)$$

where A, B, C, D_{11} , and D_{44} are expansion coefficients of the corresponding bulk material, S_1, S_2 , and S_3 represents the three pairs of surface planes of the film. δ_i is the extrapolation length, which measures the strength of the surface effect [36]. $\sigma_r = \sigma_{xx} = \sigma_{yy}$ is the epitaxial stress in the ferroelectric thin film, Q is the electrostrictive coefficient, ρ is a material parameter having the meaning of the effective mass density. E_{ext} is the applied electric field along with z axis, and E_d is the depolarization field along with z axis.

Similar to the time-dependent Ginzburg–Landau equation, one can then establish the polarization evolution equation [34],

$$K \frac{\partial P}{\partial t} = -\rho \frac{\partial^2 P}{\partial t^2} + \left\{ -AP + 4Q\sigma_r P + E_d + E_{\text{ext}} - BP^3 - CP^5 \right. \\ \left. + D_{11} \frac{\partial^2 P}{\partial z^2} + D_{44} \left(\frac{\partial^2 P}{\partial x^2} + \frac{\partial^2 P}{\partial y^2} \right) \right\}, \quad (2)$$

where K is the viscosity coefficient related to the domain-wall mobility. The divergence theorem for the electrostatic depolarization potential Φ can be written in the form,

$$\frac{\partial^2 \Phi}{\partial x^2} + \frac{\partial^2 \Phi}{\partial y^2} + \frac{\partial^2 \Phi}{\partial z^2} = \frac{1}{\alpha} \frac{\partial P}{\partial z}, \quad (3)$$

where α is the dielectric constant of the film without the effect of spontaneous polarization, then

$$E_d = -\frac{\partial \Phi}{\partial z}. \quad (4)$$

The macroscopical polarization can be written as

$$P_m = \frac{\int_V P dV}{V}. \quad (5)$$

Simulations of systems consisting of 100×100 lattices are done in three-dimensional space with two spatial coordinates ($x \times z$) and one temporal coordinate t . Periodic boundary conditions are imposed. This is reasonable when the domain size is comparable to the computational cell size [34].

By adopting a set of dimensionless variables based on Eqs. 2, 3, and 4, we obtained,

$$\begin{aligned} K \sqrt{\frac{1}{\rho|A|}} \frac{\partial \tilde{P}}{\partial \tilde{t}} = & -\frac{\partial^2 \tilde{P}}{\partial \tilde{t}^2} + \left[\left(-\frac{A}{|A|} + \frac{4Q\sigma_r}{|A|} \right) \tilde{P} + \tilde{E}_d + \tilde{E}_{\text{ext}} \right. \\ & \left. - \frac{B|P_0|^2}{|A|} \tilde{P}^3 - \frac{C|P_0|^4}{|A|} \tilde{P}^5 + \frac{\partial^2 \tilde{P}}{\partial \tilde{x}^2} + \frac{\partial^2 \tilde{P}}{\partial \tilde{z}^2} \right], \end{aligned} \quad (6)$$

$$\frac{|A|}{D_{44}} \frac{\partial^2 \Phi}{\partial \tilde{x}^2} + \frac{|A|}{D_{11}} \frac{\partial^2 \Phi}{\partial \tilde{z}^2} = \frac{|P_0|}{\alpha} \sqrt{\frac{|A|}{D_{11}}} \frac{\partial \tilde{P}}{\partial \tilde{z}}, \quad (7)$$

$$E_d = -\sqrt{\frac{|A|}{D_{11}}} \frac{\partial \Phi}{\partial \tilde{z}}, \quad (8)$$

where

$$\begin{aligned} \tilde{x} &= \sqrt{\frac{|A|}{D_{44}}} x, \quad \tilde{z} = \sqrt{\frac{|A|}{D_{11}}} z, \quad \tilde{t} = \sqrt{\frac{|A|}{\rho}} t, \quad \tilde{P} = \frac{P}{|P_0|}, \quad \tilde{E}_{\text{ext}} \\ &= \frac{E_{\text{ext}}}{|A||P_0|}, \quad \tilde{E}_d = \frac{E_d}{|A||P_0|}, \end{aligned} \quad (9)$$

where P_0 is the spontaneous polarization.

For a given external field $\tilde{E}_{\text{ext}} = \tilde{E}_0 \sin(\tilde{\omega} \tilde{t})$, the evolution of polarization, thus the polarization hysteresis loops and the initial curves of ferroelectric films can be obtained

by Eqs. 6, 7, and 8, where $\tilde{\omega} = \omega\sqrt{\rho/|A|}$ is the normalized frequency of the applied field.

Simulation results and discussions

Using the coefficients (the list of the parameters used in the calculation: $A = -4.124 \times 10^7 \text{ N m}^2/\text{C}^2$, $B = -2.097 \times 10^8 \text{ N m}^6/\text{C}^4$, $C = 3.412 \times 10^9 \text{ N m}^{10}/\text{C}^6$, $Q = 0.113 \text{ m}^4/\text{C}^2$, $\sigma_r = 1.3 \times 10^9 \text{ N/m}^2$, $D_{11} = 3.9 \times 10^{-11} \text{ N m}^4/\text{C}^2$, $D_{44} = 3.9 \times 10^{-11} \text{ N m}^4/\text{C}^2$, $P_0 = 0.963 \text{ C/m}^2$), the ferroelectric hysteresis loop, merged with the initial curve when $\tilde{\omega} = \tilde{\omega}_0 = 2\pi/6400$, $\tilde{E}_0 = 1.23 \times 10^3$ and $K/\sqrt{\rho|A|} = K_0/\sqrt{\rho_0|A|} = 3000$ are simulated, as shown in the Fig. 1. Under the applied field, the ferroelectric domains along the field direction expand, the normalized polarization \tilde{P} increases along the curve O–A–B, i.e., the initial polarization curve. Eventually, all the domains are oriented along the field direction and the system enters single-domain state at B. As the external field continues to increase, polarization derived from electron and ion polarization increases linearly with the electric field along the curve B–C. In the subsequent cycle, polarization changes with the external field along the curve C–B–D–F–G–H–I–C, which forms the ferroelectric hysteresis loop.

Figure 2a displays the influence of the normalized frequency $\tilde{\omega}$, the viscosity coefficient K and the effective mass density ρ on ferroelectric hysteresis loop and the initial curve under $\tilde{E}_0 = 1.23 \times 10^2$, in which the dotted (marked 1), dashed (marked 2) and solid (marked 3) curves correspond to the parameters $(\tilde{\omega}, K, \rho)$ of $(\tilde{\omega}_0, K_0, \rho_0)$, $(10\tilde{\omega}_0, K_0, \rho_0)$ and $(20\tilde{\omega}_0, K_0, \rho_0)$, respectively. Some other parameter groups can also induce the same curves, e. g., $(\tilde{\omega}_0, 10K_0, \rho_0)$ and $(\tilde{\omega}_0, K_0, \rho_0/100)$ present the same dashed curve as curve 2, while $(\tilde{\omega}_0, 20K_0, \rho_0)$ and $(\tilde{\omega}_0, K_0,$

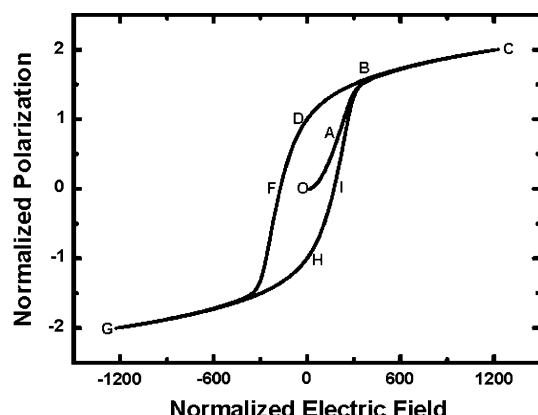


Fig. 1 The saturated ferroelectric hysteresis loop with the initial polarization curve, where $\tilde{\omega} = 2\pi/6400$, $\tilde{E}_0 = 1.23 \times 10^3$, and $K/\sqrt{\rho|A|} = 3000$

$\rho_0/400$), the same solid curves as curve 3. Obviously, the initial curve and polarization loop strongly depend on $\tilde{\omega}$, K , and ρ . Both the normalized coercive field and remanent polarization increase with the increase of $\tilde{\omega}$ and K , but decrease with the increase of ρ . Interestingly, the constant $\tilde{\omega}K/\sqrt{\rho}$ can induce the same curve and loop, and the small $\tilde{\omega}K/\sqrt{\rho}$ corresponds to the rapidly increased initial polarization curve. In order to clarify frequency bandwidth of the model, we simulate the frequency dependence of the loop under $K/\sqrt{\rho|A|} = 3000$, as shown in Fig. 2b, in which the corresponding frequencies are 0.5, 1, 2, 4, 10, 20, and $40\tilde{\omega}_0$. The inset in Fig. 2b depicts the hysteresis area $\langle A \rangle$ versus the frequency $\tilde{\omega}$. Obviously, the area increases monotonically with increase of the frequency, implying that our model is appropriate only for the low frequency

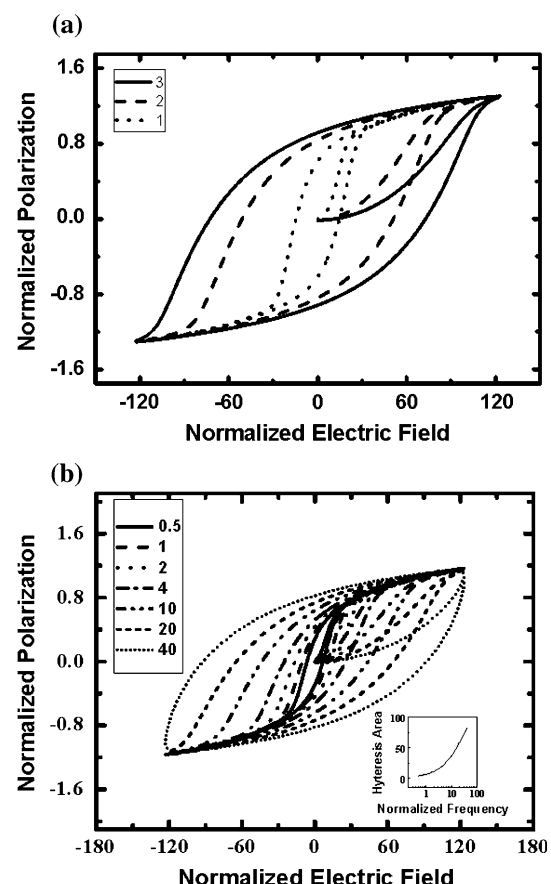


Fig. 2 **a** The normalized frequency $\tilde{\omega}$, the effective mass density ρ , and the viscosity coefficient K dependences of the hysteresis behaviors under $\tilde{E}_0 = 1.23 \times 10^2$, in which the dotted (marked 1), dashed (marked 2), and solid (marked 3) curves correspond to the results when $\tilde{\omega}K/\sqrt{\rho}$ is equal to $\tilde{\omega}_0K_0/\sqrt{\rho_0}$, $10\tilde{\omega}_0K_0/\sqrt{\rho_0}$, and $20\tilde{\omega}_0K_0/\sqrt{\rho_0}$, respectively. **b** The frequency dependence of the loop for $\tilde{E}_0 = 1.23 \times 10^2$ and $K/\sqrt{\rho|A|} = 3000$, in which the corresponding frequencies are $0.5\tilde{\omega}_0$, $\tilde{\omega}_0$, $2\tilde{\omega}_0$, $4\tilde{\omega}_0$, $10\tilde{\omega}_0$, $20\tilde{\omega}_0$, and $40\tilde{\omega}_0$. The inset in **b** depicts the hysteresis area versus the frequency

because $\langle A \rangle \propto \omega^{-1}$ as $\omega \rightarrow \infty$ in previous experimental observation [12, 13].

The viscosity of a material is used to explain some switching properties such as switching time [37, 38] and self-heating [23]. Now we can easily know from Eq. 6 that evolvement of the normalized polarization \tilde{P} approximately obeys the forced and damping oscillation. It is reasonable to consider four kinds of forces exerting on the domains during the polarization switching: the electrical force ($F_E = \tilde{E}_{\text{ext}}$), the inertia force F_I which is related to the domain “acceleration” $\partial^2 \tilde{P} / \partial t^2$, the viscous force $F_V = (K / \sqrt{\rho|A|}) \partial \tilde{P} / \partial t$ which is proportional to the domain “speed” $\partial \tilde{P} / \partial t$ and acts contrarily to the domain motion, and the restoring force (F_R) that forces the domains to come partially back to their equilibrium position. Therefore, the coercive field may be interpreted as an effective field necessary to overcome the three resistance forces ($F_R + F_V + F_I$) during the polarization switching. Consequently, the higher frequencies $\tilde{\omega}$, implying the higher “speed” and higher “acceleration”, thus the higher F_V and F_I , induces the higher coercive field. Similarly, due to $F_V \propto K / \sqrt{\rho}$, the increase in K or the decrease in ρ should produce a continuous increase in the coercive field.

It should be noted that the normalized frequency $\tilde{\omega}$ contains the factor $\sqrt{\rho}$, therefore, the form of the polarization hysteresis loops and the initial curves is determined by $\omega K / \rho$ if the other parameters are constant.

The hysteresis behaviors for various electric field amplitudes of $\tilde{E}_0 = 37, 49, 61, 74, 86, 98, 110, 123$ under $K / \sqrt{\rho|A|} = 3000$ and $\tilde{\omega} = \tilde{\omega}_0 = 2\pi/6400$ are shown in Fig. 3. The inset depicts the relation between hysteresis area $\langle A \rangle$ and electric field amplitude \tilde{E}_0 , indicating that the area $\langle A \rangle$ of the saturated loops increases with the increase of the field amplitude, which is consistent with

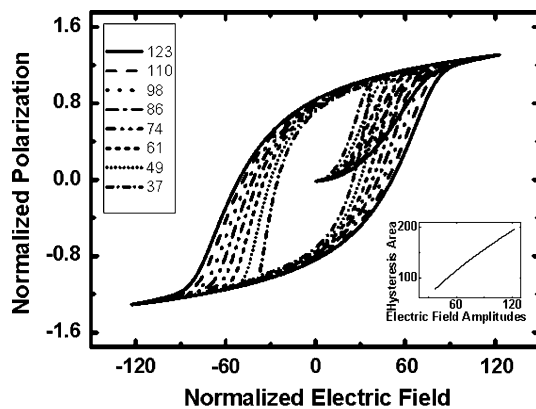


Fig. 3 The hysteresis behaviors for various electric field amplitude of $\tilde{E}_0 = 37, 49, 61, 74, 86, 98, 110, 123$ under $K / \sqrt{\rho|A|} = 3000$ and $\tilde{\omega} = 2\pi/6400$. The inset shows the relation between hysteresis area $\langle A \rangle$ and electric field amplitude \tilde{E}_0

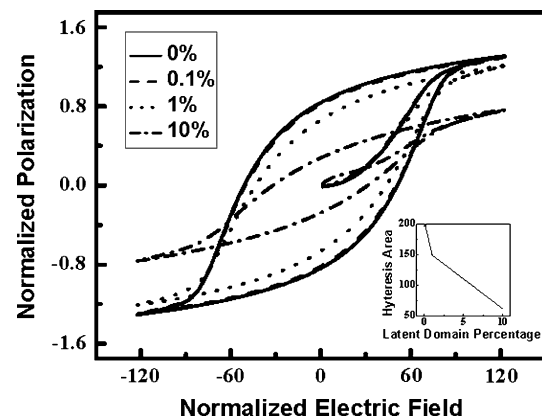


Fig. 4 The ferroelectric hysteresis behaviors under different percentages of latent domains for $\tilde{E}_0 = 1.23 \times 10^2$, $K / \sqrt{\rho|A|} = 3000$ and $\tilde{\omega} = 2\pi/6400$. The inset demonstrates the hysteresis area versus the percentage

experimental result of PZT bulk ceramic [17]. According to $\langle A \rangle \propto \tilde{E}_0^m$, our power $m \approx 0.78$.

The influence of the percentage (0, 0.1, 1, and 10%) of latent domain on the ferroelectric hysteresis loops for $K / \sqrt{\rho|A|} = 3000$ and $\tilde{\omega} = 2\pi/6400$ is obtained, as shown in Fig. 4. The inset demonstrates the hysteresis area versus the percentage, revealing that the increasing percentage results in a remarkable decrease in the remanent polarization as well as in the coercive field. It has been proposed that the increase of switching cycles leads to an increase of latent domains caused by the pinning of domain walls by defects (mainly oxygen vacancies) inside thin films during the fatigue process [39]. The latent domains do not switch with the applied field, which directly reduce the remanent polarization; on the other hand, the interaction between the switchable domains and the latent domains hampers the reorientation of the switchable domains near to the latent domains, reducing the remanent polarization.

Conclusions

In order to better understand the polarization switching mechanisms, the complete hysteresis behavior, including the polarization loops and the initial polarization curves, of ferroelectric films with 180° domain boundaries perpendicular to the film surface is simulated based on an extensive time-dependent Ginzburg–Landau model. The results display the clear dependence on the parameters (the frequency ω of the applied electric field, the effective mass density ρ and the viscosity coefficient K of the material), which implies the coercive field may be governed by the restoring force, the viscous force and the inertia force, and the constant $\omega K / \rho$ can induce the same curve and loop. In addition, we indicate that the increasing percentage of

latent domains leads to a remarkable decrease in the remanent polarization as well as in the coercive field, which is consistent with the fatigue mechanism.

Acknowledgements The authors are grateful for the financial supports by the 973 program (2007CB616910), the NSFCs (50572021, 10774036, and 60876055), the NSFs of Hebei Province (E2008000620, E2008000631), State Education Ministry (207013), The Key Laboratory on Photoelectric Information Materials of Hebei province, and foundation of Hebei University.

References

- Wu J, Wang J (2010) *Acta Mater* 58:1688
- Auciello O, Scott JF, Ramesh R (1998) *Phys Today* 51:22
- Dawber M, Rabe KM, Scott JF (2005) *Rev Mod Phys* 77:1083
- Chou U, Jang HM, Kim MG, Chang CH (2002) *Phys Rev Lett* 89:087601
- Liu BT, Yan XB, Zhang X, Cheng CS, Li F, Bian F, Zhao QX, Guo QL, Wang YL, Li XH, Zhang XY, Li CR, Wang YS (2007) *Appl Phys Lett* 91:142908
- Wang YL, Wang XY, Chu LZ, Deng ZC, Liang WH, Liu BT, Fu GS, Wongdamnern N, Sareein T, Yimnirun R (2009) *Phys Lett A* 373:4282
- Wang XY, Wang YL, Yang RJ (2009) *Appl Phys Lett* 95:142910
- Wang YL, Wu ZH, Deng ZC, Chu LZ, Liu BT, Liang WH, Fu GS (2009) *Ferroelectrics* 386:133
- Spaldin NA, Fiebig M (2005) *Science* 309:391
- Cheng J, Yu S, Chen J, Meng Z, Cross LE (2006) *Appl Phys Lett* 89:122911
- Scott JF, Galt D, Price JC, Beall JA, Ono RH, Araujo CAP, McMillan LD (1995) *Integr Ferroelectr* 6:189
- Guyomar D, Ducharme B, Sebald G (2007) *J Phys D Appl Phys* 40:6048
- Guyomar D, Ducharme B, Sebald G (2010) *J Appl Phys* 107:114108
- Lente MH, Picinin A, Rino JP, Eiras JA (2004) *J Appl Phys* 95:2646
- So YW, Kim DJ, Noh TW, Yoon J-G, Song TK (2005) *Appl Phys Lett* 86:092905
- Lohse O, Grossmann M, Boettger U, Bolten D, Waser R (2001) *J Appl Phys* 89:2332
- Yimnirun R, Laosiritaworn Y, Wongsaenmai S, Ananta S (2006) *Appl Phys Lett* 89:162901
- Jiang QY, Subbarao EC, Cross LE (1994) *J Appl Phys* 75:7433
- Okazaki K, Sakata K (1962) *Electrotech J Jpn* 7:13
- Lambeck PV, Jonker GH (1978) *Ferroelectrics* 22:729
- Warren WL, Pike GE, Vanheusden K, Dimos D, Tuttle BA (1996) *J Phys Soc Jpn* 79:9250
- Cohen RE (2000) *J Phys Chem Solids* 61:139
- Lente MH, Eiras JA (2000) *J Phys Condens Matter* 12:5939
- Lente MH, Eiras JA (2001) *J Appl Phys* 89:5093
- Lente MH, Eiras JA (2002) *J Appl Phys* 92:2112
- Scott JF, Dawber M (2000) *Appl Phys Lett* 76:3801
- Dawber M, Scott JF (2001) *Integr Ferroelectr* 32:259
- Jung DJ, Dawber M, Scott JF, Sinnamon LJ, Bregg JM (2002) *Integr Ferroelectr* 48:59
- Chen L, Roytburd AL (2007) *Appl Phys Lett* 90:102903
- Miller SL, Schwank JR, Nasby RD, Rodgers MS (1991) *J Appl Phys* 70:2849
- Vendik OG, Razumov SV, Tumarkin AV, Nikol'skii MA, Gaidukov MM, Gagarin AG (2005) *Appl Phys Lett* 86:022902
- Ye Z, Tang MH, Zhou YC, Zheng XJ, Cheng CP, Hu ZS, Hu HP (2007) *Appl Phys Lett* 90:042902
- Zhang J, Tang MH, Tang J, Yang XF, Xu HY, Zhao WF, Zheng XJ, Zhou YC (2007) *Appl Phys Lett* 91:162908
- Wang B, Xia R, Fan H, Woo CH (2003) *J Appl Phys* 94:3384
- Ganpule CS, Roytburd AL, Nagarajan V, Hill BK, Ogale SB, Williams ED, Ramesh R (2001) *Phys Rev B* 65:014101
- Zhong WL, Wang YG, Zhang PL, Qu BD (1994) *Phys Rev B* 50:698
- Ishibashi Y (1990) *J Phys Soc Jpn* 59:4148
- Mitoseriu L, Ricinschi D, Harnagea C, Okuyama M, Tsukamoto T, Tura V (1996) *Jpn J Appl Phys* 35:5210
- Li W, Chen A, Lu XM, Zhu JS, Wang YN (2005) *Appl Phys Lett* 86:192908